Thermodynamic properties at the kinetic freeze-out in the Au+Au and Cu+Cu collisions at the RHIC using the Tsallis distribution*

Wei-Hao Wu,[1] Jun-Qi Tao,[2] Hua Zheng [1,†] Wen-Chao Zhang,[1] Xing-Quan Liu [3] Li-Lin Zhu,[4] and Aldo Bonasera[5,6]

[1] *School of Physics and Information Technology, Shaanxi Normal University, Xi'an 710119, China*
[2] *Key Laboratory of Quark & Lepton Physics (MOE) and Institute of Particle Physics, Central China Normal University, Wuhan 430079, China*
[3] *Institute of Nuclear Science and Technology, Sichuan University, Chengdu 610064, China*
[4] *Department of Physics, Sichuan University, Chengdu 610064, China*
[5] *Cyclotron Institute, Texas A&M University, College Station, TX 77843, USA*
[6] *Laboratori Nazionali del Sud, INFN, 95123 Catania, Italy*

The thermodynamic properties of charged particles, such as the energy density, pressure, entropy density, particle density, and squared speed of sound at the kinetic freeze-out in the $\mathrm{Au}+\mathrm{Au}$ collisions from the relativistic heavy ion collider (RHIC) beam energy scan program ($\sqrt{s_{\mathrm{NN}}}$=7.7–200 GeV) and in the $\mathrm{Cu}+\mathrm{Cu}$ collisions at $\sqrt{s_{\mathrm{NN}}}$=62.4, 200 GeV are studied using the thermodynamically consistent Tsallis distribution. The energy density, pressure, and particle density decrease monotonically with the collision energy for the same collision centrality; These properties also decrease monotonically from the central to peripheral collisions at the same collision energy. While the scaled energy density ε/T^4 and scaled entropy density s/T^3 demonstrate the opposite trend with the collision energy for the same collision centrality. There is a correlation between ε/T^4 and s/T^3 at the same centrality. In addition, the squared speed of sound was calculated to determine that all the collision energies share nearly the same value at different collision centralities.

Keywords: Heavy-ion collision, Tsallis distribution, Kinetic freeze-out, Energy density, Entropy density, Particle density, Squared speed of sound, Pressure

I. INTRODUCTION

In relativistic heavy-ion collisions, an extremely hot and dense mixture of quarks and gluons is created, which is called the quark gluon plasma (QGP) [1–8]. The QGP can only exist for a significantly short time and hadronizes into mesons and baryons owing to its color confinement. These particles interact with one another or form light nuclei and continue expanding. The system cools and reaches the chemical freeze-out point when the abundances of all the particle species are unchanged. The system continues evolving to reach a kinetic freeze-out, where the distributions of all the particles do not change. Subsequently, the information of particles are recorded by detectors set around the collision region. With the measured information, such as the multiplicities of the particles and particle transverse momentum (p_T) spectra, the properties of the QGP and the system can be studied at different evolution stages.

In previous experimental and theoretical studies, several statistical distributions or models based on different assumptions have been used to describe the particle transverse momentum spectra and to extract relevant information about the collision system. These include the Boltzmann-Gibbs (BG) distribution, Fermi-Dirac distribution, Bose-Einstein distribution, double exponential distribution, m_T-exponential distribution [9, 10], Erlang distribution [11], multi-source model [12], blast-wave model [13], Tsallis distribution [14–26], and the Generalized Fokker-Planck Solution (GFPS) [27, 28], etc. As a generalization of the BG distribution, the Tsallis distribution has been recently highly valued [17–23, 26]. This is ascribed to its successful application in describing the particle p_{T} spectra in the $\mathrm{p}+\mathrm{p}$ collisions (the transverse momentum spans two orders of magnitude and the yield spans 15 orders of magnitude) presented by Wong *et al.* [14, 15] and in several other studies [16, 19, 24, 25] dedicated to describing the particle transverse momentum spectra produced in the pp, pA, and AA collisions. Cleymans *et al.* demonstrated the thermodynamic consistency of the Tsallis distribution. Utilizing the Tsallis distribution, Azmi *et al.* [24] described the transverse momentum spectra of charged particles produced in the $\mathrm{Pb}+\mathrm{Pb}$ collisions at the Large Hadron Collider (LHC) and deduced the thermodynamic properties of the collision system at the kinetic freeze-out. Combined with the thermodynamic properties of the system at the chemical freeze-out point obtained by fitting the particle yields using the statistical model, this can provide an evolutionary picture of the thermodynamic quantities for the hadronic phase from the chemical to kinetic freeze-out point [24].

In this study, following Ref. [24], with the experimental data of the Au+Au collisions from the beam energy scan (BES) program published by the STAR Collaboration ($\sqrt{s_{\mathrm{NN}}} = 7.7 - 200$ GeV) [29–31], and data of the $\mathrm{Cu}+\mathrm{Cu}$ collisions at $\sqrt{s_{\mathrm{NN}}} = 62.4, 200$ GeV [32, 33] measured by the PHOBOS Collaboration, the transverse momentum spectra of the charged particles at the RHIC were systematically studied using the thermodynamically consistent Tsallis distribution. The nonextensive parameter q as well as the temperature parameter T were extracted in the Tsallis distribution. Subsequently, we investigated the thermodynamic prop-

* This work was supported in part by the National Natural Science Foundation of China (Nos. 11905120 and 11947416), the Natural Science Foundation of the Sichuan Province (No. 2023NSFSC1322), the United States Department of Energy (# DE-FG02-93ER40773), and the NNSA (No. DENA0003841 (CENTAUR)).

† Corresponding author, zhengh@snnu.edu.cn

erties of the charged particles at the kinetic freeze-out, that is, the energy density, pressure, entropy density, particle density, and squared speed of sound. The dependence of the thermodynamic quantities on the collision energy, system size, and centrality was also studied and discussed.

The remainder of this paper is organized as follows. The Tsallis distribution for the transverse momentum spectrum of the charged particles as well as the formulas for the thermodynamic quantities are briefly introduced in Section II, along with the fitting results of the experimental transverse momentum spectra of the charged particles. The thermodynamic quantities of the Au+Au and Cu+Cu collisions were calculated at different collision energies and centralities, the results of which are discussed in Section III. A brief summary is given in section IV.

II. TSALLIS DISTRIBUTION

The Tsallis distribution is a generalization of the Boltzmann-Gibbs distribution in classical thermodynamics, which was proposed by Tsallis [34]. Within the framework of the thermodynamically consistent Tsallis distribution, the momentum distribution of the final particles produced in relativistic heavy-ion collisions can be expressed as follows:

$$\frac{d^2N}{2\pi p_\mathrm{T}\mathrm{d}p_\mathrm{T}\mathrm{d}y} = gVE\frac{1}{(2\pi)^3}\left[1+(q-1)\frac{E-\mu}{T}\right]^{-\frac{q}{q-1}}. \tag{1}$$

Here, g indicates the degeneracy of the particles, V is the volume, E is the energy, μ is the chemical potential, q is the Tsallis parameter, and T is the temperature parameter. Equation (1) can be expressed as follows [18, 24, 35, 36]:

$$\frac{d^2N}{2\pi p_\mathrm{T}\mathrm{d}p_\mathrm{T}\mathrm{d}y} = gV\frac{m_\mathrm{T}\cosh y}{(2\pi)^3} \times\left[1+(q-1)\frac{m_T\cosh y-\mu}{T}\right]^{-\frac{q}{q-1}} \tag{2}$$

in terms of the transverse momentum p_T, the transverse mass $m_\mathrm{T}=\sqrt{p_\mathrm{T}^2+m^2}$ and the rapidity y.

The majority of the charged particles are $\pi^+(\pi^-)$ mesons, and the number of positive and negative π mesons are equal in the heavy-ion collisions at the RHIC and LHC, which implies despite the collision energy being as low as 7.7 GeV, which is the lowest collision energy in the BES. However, the numbers of p and $\bar{p}$ are different, which leads to a nonzero chemical potential of the baryons. Considering that only a small portion of the charged particles are baryons, it is a sufficient approximation for assuming that the chemical potential of the particles is zero. The variations owing to the approximation of the zero chemical potential were determined to be small; our conclusions do not depend on the approximation. When only the particles in mid-rapidity ($y\approx 0$) are considered, Eq. (2) is reduced to the following:

$$\left.\frac{d^2N}{2\pi p_\mathrm{T}\mathrm{d}p_\mathrm{T}\mathrm{d}y}\right|_{y=0} = gV\frac{m_\mathrm{T}}{(2\pi)^3}\left[1+(q-1)\frac{m_\mathrm{T}}{T}\right]^{-\frac{q}{q-1}}. \tag{3}$$

In the experimental distribution of the charged particles in relativistic heavy-ion collisions, pseudorapidity η is occasionally used instead of rapidity y. The conversion from rapidity to pseudorapidity is given by the following:

$$\frac{\mathrm{d}y}{\mathrm{d}\eta} = \sqrt{1-\frac{m^2}{m_\mathrm{T}^2\cosh^2 y}}. \tag{4}$$

According to Eqs. (3, 4), the pseudorapidity distribution of the particles at mid-rapidity is as follows:

$$\left.\frac{d^2N}{2\pi p_\mathrm{T}\mathrm{d}p_\mathrm{T}d\eta}\right|_{y=0} = gV\frac{p_\mathrm{T}}{(2\pi)^3}\left[1+(q-1)\frac{m_\mathrm{T}}{T}\right]^{-\frac{q}{q-1}}. \tag{5}$$

As indicated in Ref. [24], the transverse momentum spectrum of the charged particles consists of three Tsallis distributions including pions, Kaons, and protons, by considering that the main charged particles are $\pi^+(\pi^-)$, $K^+(K^-)$, and $p(\bar{p})$, respectively, in the relativistic heavy ion collisions. Therefore, the transverse momentum distribution of the charged particles at mid-rapidity can be expressed as follows:

$$\frac{d^2N_{ch}}{2\pi p_\mathrm{T}\mathrm{d}p_\mathrm{T}\mathrm{d}\eta} = 2V\frac{p_\mathrm{T}}{(2\pi)^3}\sum_{i=1}^{3}g_i\left[1+(q-1)\frac{m_{T,i}}{T}\right]^{-\frac{q}{q-1}}, \tag{6}$$

where $i=\pi^+, K^+, p$. $m_{T,i}$ is the transverse mass of particle i in the sum of Eq. (6). Factor 2 on the right-hand side considers the contributions from the antiparticles, which is reasonable at the LHC because the multiplicities of the particles and antiparticles are equal [24]. The degeneracy factors g of the particles are $g_\pi^+=g_K^+=1, g_p=2$. However, the experimental data demonstrates significant differences between the multiplicities of the particles and antiparticles for kaons and protons at the RHIC, particularly at lower collision energies. By considering the aforementioned, we determined the effective degeneracy factor of the particles. This factor is determined by taking half the sum of one and the multiplicity ratio between the antiparticles and particles for each type of particle from the experimental data of the RHIC [9, 10, 33, 37]. These values are listed in Table 1.

The formulas for the thermodynamic quantities at the kinetic freeze-out in the thermodynamically consistent Tsallis statistics are as follows [24, 38]:

$$\varepsilon = 2\sum_{i=1}^{3}g_i\int\frac{d^3p}{(2\pi)^3}E_i\left[1+(q-1)\frac{E_i}{T}\right]^{-\frac{q}{q-1}}, \tag{7}$$

$$n = 2\sum_{i=1}^{3}g_i\int\frac{d^3p}{(2\pi)^3}\left[1+(q-1)\frac{E_i}{T}\right]^{-\frac{q}{q-1}}, \tag{8}$$

$$s = 2\sum_{i=1}^{3}g_i\int\frac{d^3p}{(2\pi)^3}\left[\frac{E_i}{T}\left(1+(q-1)\frac{E_i}{T}\right)^{-\frac{q}{q-1}} +\left(1+(q-1)\frac{E_i}{T}\right)^{-\frac{1}{q-1}}\right], \tag{9}$$

Table 1. The effective values of g_{π^+}, g_{K^+}, and g_p are used to fit the charged particle transverse momentum spectra in the Au + Au collisions at $\sqrt{s_{\rm NN}} = 7.7 - 200$ GeV and in the Cu + Cu collisions at $\sqrt{s_{\rm NN}} = 62.4, 200$ GeV. The data are obtained from Refs. [9, 10, 33, 37].

System	$\sqrt{s_{\rm NN}}$ (GeV)	g_{π^+}	g_{K^+}	g_p
Au+Au	7.7	1	1.370/2	1.007
	11.5	1	1.494/2	1.033
	14.5	1	1.558/2	1.064
	19.6	1	1.637/2	1.122
	27	1	1.728/2	1.189
	39	1	1.783/2	1.320
	62.4	1	1.860/2	1.469
	130	1	1.923/2	1.708
	200	1	1.965/2	1.769
Cu+Cu	62.4	1	1.890/2	1.480
	200	1	1.980/2	1.780

$$P = 2\sum_{i=1}^{3} g_i \int \frac{d^3p}{(2\pi)^3}\frac{p^2}{3E_i}\left[1+(q-1)\frac{E_i}{T}\right]^{-\frac{q}{q-1}}, \quad (10)$$

$$C_s^2(T) = \left(\frac{\partial P}{\partial \varepsilon}\right)_V = \frac{s}{C_V}, \quad (11)$$

$$C_V = 2\sum_{i=1}^{3} g_i \frac{q}{T^2}\int \frac{d^3p}{(2\pi)^3}E_i\left[1+(q-1)\frac{E_i}{T}\right]^{\frac{1-2q}{q-1}}, \quad (12)$$

where $i = \pi^+, K^+, p$.

To understand the behavior of the thermodynamic quantities, the analytical formulas derived for the massless particles and zero chemical potential in the Tsallis statistics are utilized for an estimation. They are provided in Ref. [39]:

$$\varepsilon = g\frac{3T^4}{\pi^2}\frac{1}{(2-q)(3-2q)(4-3q)}, \quad (13)$$

$$n = g\frac{T^3}{\pi^2}\frac{1}{(2-q)(3-2q)}, \quad (14)$$

$$s = g\frac{4T^3}{\pi^2}\frac{1}{(2-q)(3-2q)(4-3q)}, \quad (15)$$

$$P = g\frac{T^4}{\pi^2}\frac{1}{(2-q)(3-2q)(4-3q)}, \quad (16)$$

where g is the particle degeneracy factor.

Prior to calculating the thermodynamic quantities for the Au+Au and Cu+Cu collisions at the kinetic freeze-out at the RHIC using Eqs. (7, 8, 9, 10, and 11), the Tsallis parameter q and temperature parameter T need to be obtained. To achieve these parameters, we fitted the transverse momentum spectra of the charged particles for the Au+Au and Cu+Cu collisions at $\sqrt{s_{\rm NN}} = 200$ GeV for different collision centralities using Eq. (6). The results are presented in Fig. 1. The Tsallis distribution describes the transverse momentum spectra of the charged particles with momentum values lower than 8 GeV/c. The fit/data were obtained to characterize the fit quality, as shown in the bottom panels of Fig. 1, which demonstrates that most of the fit/data points fluctuated within 20%, and only a few data points where p_T was either close to 0 GeV/c or close to 8 GeV/c fluctuated within 30%. The corresponding χ^2/NDF for the fit are also listed in Tables 2 and 3, respectively. The fit quality of the peripheral collisions was better than that of the central collisions, which is consistent with our previous results [27, 28, 40–42]. The transverse momentum spectra of the charged particles from the Au+Au collisions in the BES program at $\sqrt{s_{\rm NN}} = 7.7 - 130$ GeV and the Cu+Cu collisions at $\sqrt{s_{\rm NN}} = 62.4$ GeV were also fitted with Eq. (6) and similar results were obtained as shown in Fig. 1.

Tables 2 and 3 list the temperature parameter T and Tsallis parameter q obtained by fitting the transverse momentum spectra of the charged particles from the Au+Au collisions at $\sqrt{s_{NN}} = 7.7 - 200$ GeV and Cu+Cu collisions at $\sqrt{s_{NN}} = 62.4, 200$ GeV. As reported in Ref. [25], for a given collision energy, as the collision centrality increases, that is, from the most central to peripheral collisions, the temperature parameter T demonstrates a significant decreasing trend while the Tsallis parameter q demonstrates an increasing trend; however, the absolute magnitude of the increase is significantly small. Similarly, for a given collision centrality, the temperature parameter T exhibits a decreasing trend as the collision energy increases, whereas the Tsallis parameter q displays the opposite trend.

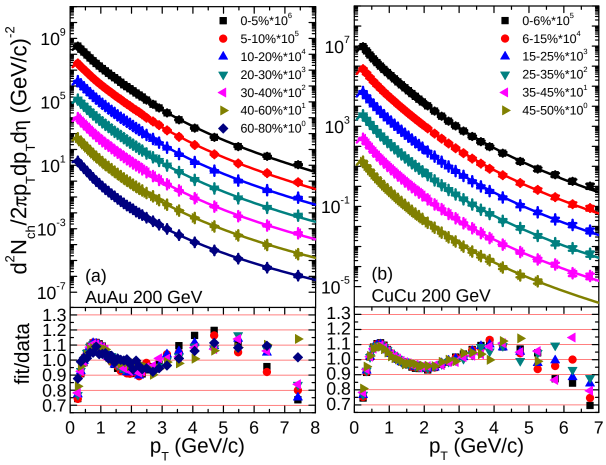

Fig. 1. (Color online) Transverse momentum spectra of the charged particles in the Au + Au (left panel) and Cu + Cu (right panel) collisions at $\sqrt{s_{NN}} = 200$ GeV measured by the STAR Collaboration and the PHOBOS Collaboration, respectively. The curves indicate fits using the Tsallis distribution Eq. (6), and the values of the degeneracy factor are obtained from Table 1. The lower panels of the figure demonstrate the values of the fit over the data. The experimental data are obtained from Refs. [31, 32].

Table 2. The values of q, T, and χ^2/NDF are obtained by using Eq. (6) to fit the transverse momentum spectra of the charged particles from the $\mathrm{Au+Au}$ collisions at $\sqrt{s_{NN}} = 7.7 - 200$ GeV. The values of the degeneracy factor are from Table 1 and the experimental data are obtained from Refs. [29–31].

System	$\sqrt{s_{NN}}$ (GeV)	Centrality	q	T (MeV)	χ^2/NDF
Au+Au	7.7	0-5%	1.0243±0.0018	183.9±3.0	28.17/38
		5-10%	1.0249±0.0020	181.9±3.3	26.70/37
		10-20%	1.0233±0.0017	181.6±3.1	29.93/38
		20-40%	1.0241±0.0018	174.1±3.1	24.58/38
		40-60%	1.0281±0.0025	155.8±3.7	13.61/36
		60-80%	1.0252±0.0031	142.8±4.3	9.21/35
Au+Au	11.5	0-5%	1.0259±0.0014	177.9±2.7	45.47/39
		5-10%	1.0277±0.0015	174.8±2.7	37.97/39
		10-20%	1.0266±0.0014	174.7±2.7	43.35/39
		20-40%	1.0284±0.0015	167.6±2.8	38.30/38
		40-60%	1.0306±0.0017	154.7±2.9	26.86/38
		60-80%	1.0315±0.0023	139.8±3.4	16.87/36
Au+Au	14.5	0-5%	1.0285±0.0014	172.8±2.7	44.44/39
		5-10%	1.0282±0.0014	172.8±2.7	51.39/39
		10-20%	1.0307±0.0014	168.1±2.7	40.69/39
		20-40%	1.0299±0.0013	165.8±2.6	52.60/39
		40-60%	1.0340±0.0015	151.6±2.7	38.48/38
		60-80%	1.0357±0.0019	137.5±2.9	25.16/37
Au+Au	19.6	0-5%	1.0316±0.0012	169.0±2.5	49.10/40
		5-10%	1.0313±0.0012	169.4±2.5	56.09/40
		10-20%	1.0323±0.0012	167.3±2.4	55.14/40
		20-40%	1.0333±0.0011	163.2±2.4	63.14/40
		40-60%	1.0374±0.0013	150.6±2.5	53.47/39
		60-80%	1.0420±0.0016	134.6±2.6	30.10/38
Au+Au	27	0-5%	1.0359±0.0011	165.3±2.3	51.86/42
		5-10%	1.0362±0.0011	165.1±2.3	56.09/41
		10-20%	1.0375±0.0011	163.2±2.3	55.10/41
		20-40%	1.0390±0.0010	159.2±2.2	59.06/41
		40-60%	1.0441±0.0012	146.6±2.3	48.50/40
		60-80%	1.0489±0.0014	131.9±2.4	33.02/39
Au+Au	39	0-5%	1.0426±0.0009	160.2±2.0	40.46/44
		5-10%	1.0434±0.0009	159.5±2.1	43.44/44
		10-20%	1.0444±0.0009	158.4±2.0	44.75/44
		20-40%	1.0471±0.0009	153.6±2.0	48.87/45
		40-60%	1.0513±0.0010	143.4±2.1	44.45/43
		60-80%	1.0552±0.0011	130.7±2.2	43.40/41
Au+Au	62.4	0-5%	1.0521±0.0010	151.8±2.2	31.39/44
		5-10%	1.0533±0.0010	150.8±2.2	29.68/44
		10-20%	1.0547±0.0009	149.3±2.1	31.69/44
		20-40%	1.0582±0.0009	143.8±2.0	28.62/44
		40-60%	1.0635±0.0010	133.2±2.1	28.48/44
		60-80%	1.0690±0.0012	120.0±2.2	25.56/43
Au+Au	130	0-5%	1.0702±0.0026	132.5±3.7	20.09/27
		5-10%	1.0730±0.0027	129.8±3.7	21.15/27
		10-20%	1.0760±0.0028	126.7±3.7	18.71/27
		20-30%	1.0809±0.0026	120.8±3.4	14.64/27
		30-40%	1.0807±0.0027	119.4±3.5	17.64/27
		40-60%	1.0903±0.0024	106.3±3.0	15.85/27
		60-80%	1.0976±0.0025	94.2±2.9	10.06/27
Au+Au	200	0-5%	1.0786±0.0009	122.7±1.6	101.40/29
		5-10%	1.0791±0.0011	122.1±1.8	82.34/29
		10-20%	1.0828±0.0010	118.6±1.6	76.00/29
		20-30%	1.0854±0.0010	116.4±1.6	60.71/29
		30-40%	1.0884±0.0011	112.6±1.7	62.07/29
		40-60%	1.0945±0.0010	104.0±1.6	32.50/29
		60-80%	1.1028±0.0011	91.3±1.5	21.85/29

III. THERMODYNAMIC VARIABLES

In this section, the temperature parameter T and Tsallis parameter q listed in Tables 2 and 3 are used to calculate the thermodynamic quantities for relativistic heavy-ion collisions

Table 3. The values of q, T, and χ^2/NDF are obtained by using Eq. (6) to fit the transverse momentum spectra of the charged particles from the Cu + Cu collisions at $\sqrt{s_{NN}} = 62.4, 200$ GeV. The values of the degeneracy factor are from Table 1 and the experimental data are obtained from Refs. [32, 33].

System	$\sqrt{s_{NN}}$ (GeV)	Centrality	q	T (MeV)	χ^2/NDF
Cu+Cu	62.4	0-6%	1.0623±0.0024	126.6±3.7	26.07/26
		6-15%	1.0637±0.0024	125.0±3.6	26.40/26
		15-25%	1.0694±0.0024	118.2±3.5	19.17/26
		25-35%	1.0694±0.0026	117.2±3.7	21.74/26
		35-40%	1.0718±0.0027	113.3±3.7	19.42/26
Cu+Cu	200	0-6%	1.0838±0.0021	115.8±3.3	19.54/30
		6-15%	1.0861±0.0021	113.3±3.3	17.28/30
		15-25%	1.0894±0.0021	109.8±3.2	14.75/30
		25-35%	1.0914±0.0021	107.2±3.2	12.92/30
		35-45%	1.0938±0.0022	103.6±3.2	12.26/30
		45-50%	1.0973±0.0024	99.0±3.4	9.61/30

within the framework of the thermodynamically consistent Tsallis statistics. The errors propagated by the uncertainties of the fitting parameters are also considered. Note, the thermodynamic quantities are calculated for the charged particles at the kinetic freeze-out hereafter.

A. Energy density

The energy densities for different centralities at various collision energies were calculated using Eq. (7). The energy densities ε in units of GeV/fm^3 are shown in Fig. 2a as a function of centrality. In this study, 0 represents the most central collision, and 1 represents the most peripheral collision. The results for the Pb+Pb collisions with collision energies at $\sqrt{s_{NN}} = 2760$, 5020 GeV obtained from Ref. [24] are also shown in the figure. Our results demonstrate that the energy density of the collision system decreases from the central to peripheral collisions. The energy density decreases as the collision energy increases for a collision system with a similar size at a given collision centrality. The size dependence of the system can also be observed by comparing the results from the Cu+Cu and Au+Au collisions at the same collision energy and centrality. This may be owing to the fact that the atomic number of copper is smaller than that of gold, leading to a Cu+Cu collision system with less stopping power, which is more prone to expansion than that of the Au+Au. Similar results are observed for the pressure and particle density, as shown in Fig. 3a and Fig. 6, respectively. According to the results, there is an apparent interplay between the total multiplicity of the charged particles produced in the collisions associated with the collision energy and the expansion of the collision system related to the volume of the system. A higher energy of the collision system results in a larger volume at the kinetic freeze-out, which results in a smaller density at the same collision centrality, leading to a low energy density, pressure, and particle density for high collision energies [43]. The only exception was for the Pb+Pb collisions at $\sqrt{s_{\mathrm{NN}}} = 2760$ GeV at the LHC. The total multiplicity of the charged particles must increase faster than the volume for the Pb+Pb collisions from $\sqrt{s_{\mathrm{NN}}} = 2760$ GeV to 5020 GeV.

For comparison, we determined the chemical freeze-out energy density values for the collision systems analyzed in our study. Zhang and Xu [44] obtained the chemical freeze-out energy densities of mid-central collisions at $\sqrt{s_{\mathrm{NN}}}$=7.7, 14.5, 19.6, 27, and 39 GeV using the baryon chemical potential and the temperature extracted from the statistical model; the densities were 0.49, 0.62, 0.68, 0.69, and 0.69 GeV/fm^3, respectively. These energy densities during the chemical freeze-out were much higher than the kinetic freeze-out previously indicated. This can be demonstrated by Eq. (13), which indicates that the energy density of massless particles is proportional to the fourth power of the temperature, and the temperature at the chemical freeze-out is higher than that at the kinetic freeze-out. Thus, the results are consistent with the evolution of the relativistic heavy-ion collision systems.

Figure 2b demonstrates the scaled energy density ε/T^4 versus the centrality. The results of ε/T^4 for the Pb+Pb collisions at $\sqrt{s_{\mathrm{NN}}} = 2760, 5020$ GeV obtained from Ref. [24] are also presented in the figure. The dependence of the scaled energy density on the centrality appears to exhibit a marked reducuction because the kinetic freeze-out temperature T_{kin} strongly depends on the centrality [43]. The system size dependence of the scaled energy density nearly disappeared in the collision system when the results for the Au+Au and Cu+Cu collisions at the same collision energy were compared. In addition, the values of ε/T^4 demonstrate an increasing trend as a function of the collision energy.

B. Pressure and squared speed of sound

In the current analysis, the pressure at the kinetic freeze-out can be obtained from Eq. (10). In Fig. 3a, the pressure, which is in units of GeV/fm^3, demonstrates a significant and expected increase from the peripheral to the central collisions for a given collision energy. The pressure results for the Pb+Pb collisions at $\sqrt{s_{\mathrm{NN}}}$=2760, 5020 GeV obtained from Ref. [24] are also shown in the figure. The pressure exhibited the same pattern as the particle density, as shown in

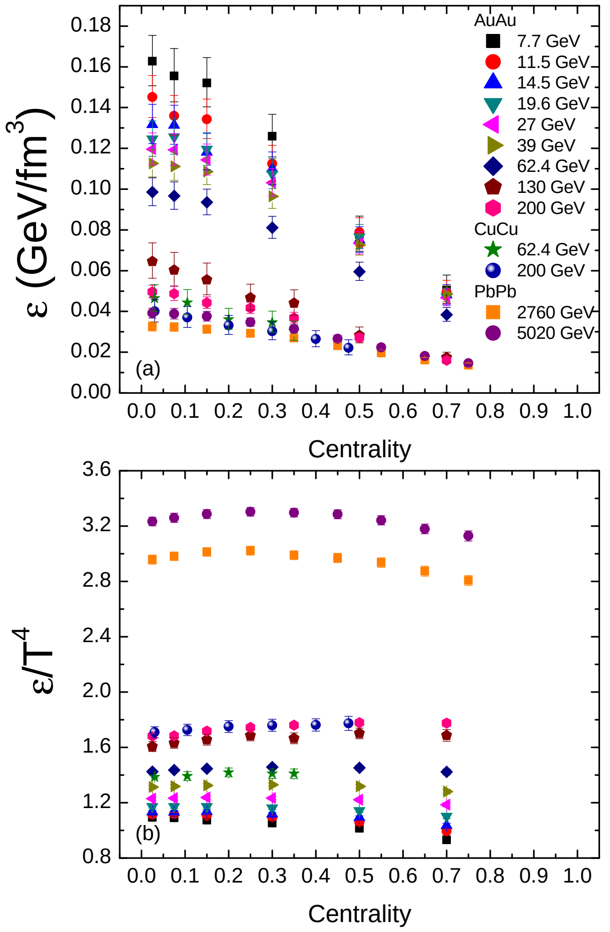

Fig. 2. (Color online) Energy density and the scaled energy density ε/T^4 in the Au+Au collisions at $\sqrt{s_{NN}} = 7.7 - 200$ GeV, and in the Cu+Cu collisions at $\sqrt{s_{NN}} = 62.4, 200$ GeV, as a function of centrality. The values are calculated by Eq. (7). The results for the Pb+Pb collisions are obtained from Ref. [24].

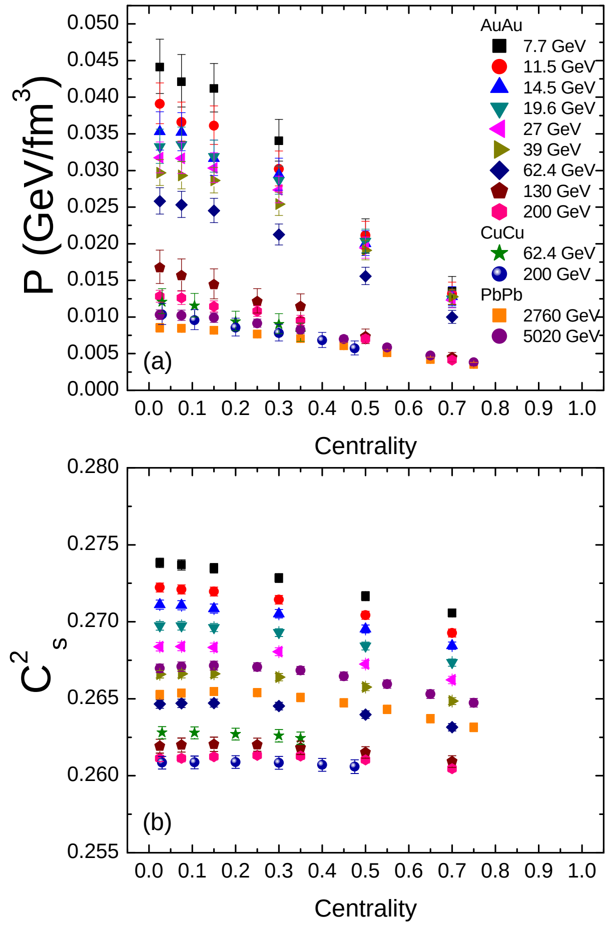

Fig. 3. (Color online) The pressure and squared speed of sound in the Au+Au collisions at $\sqrt{s_{\rm NN}} = 7.7 - 200$ GeV, and in the Cu+Cu collisions at $\sqrt{s_{\rm NN}} = 62.4, 200$ GeV, as a function of centrality. The pressure values are calculated using Eq. (10) and those of the squared speed of sound are calculated using Eqs. (11, 12). The pressure results for the Pb+Pb collisions are obtained from Ref. [24].

Fig. 6. See the explanation in section III A for further details.

The squared speed of sound can be calculated using Eqs. (11, 12); the results are shown in Fig. 3b. The parameters used to calculate the squared speed of sound for the Pb+Pb collisions were obtained from Ref. [24]. The values of the squared speed of sound are approximately between 0.26 to 0.275 for all the collision energies and centralities. The value for massless ideal gas is 1/3, which is the upper limit. The values of the squared speed of sound demonstrate a significantly small decreasing trend, with the collision centrality varying from the central to peripheral collisions at the same collision energy.

C. Entropy density

Entropy is a particularly important quantity in statistics. The values calculated using Eq. (9) are presented in Fig. 4, where the entropy density is scaled by T^3. The s/T^3 values for the Pb+Pb collisions at $\sqrt{s_{\rm NN}}$=2760, 5020 GeV, obtained from Ref. [24], are shown in the insert. Similar to the scaled energy densities shown in Fig. 2b, the scaled entropy density presents a significantly weak centrality dependence for a given collision energy. No system size effect was observed for the Cu+Cu and Au+Au collisions. Furthermore, the values of s/T^3 generally increased as the collision energy increased.

The thermodynamic relationship was also verified explicitly:

$$\varepsilon + P = Ts \tag{17}$$

which holds.

As illustrated in Fig. 5, the scaled ε/T^4 and s/T^3 are plotted for the most central collisions (0-5% or 0-6%) and for the most peripheral collisions (60-80%) from 7.7 to 5020 GeV as a function of $\ln(s_{NN})$. The scaled ε/T^4 and s/T^3 as a function of the centrality demonstrate the same trend. The data points were fit with power-law functions, as indicated by the lines in the figure. The curves were similar and the fitting

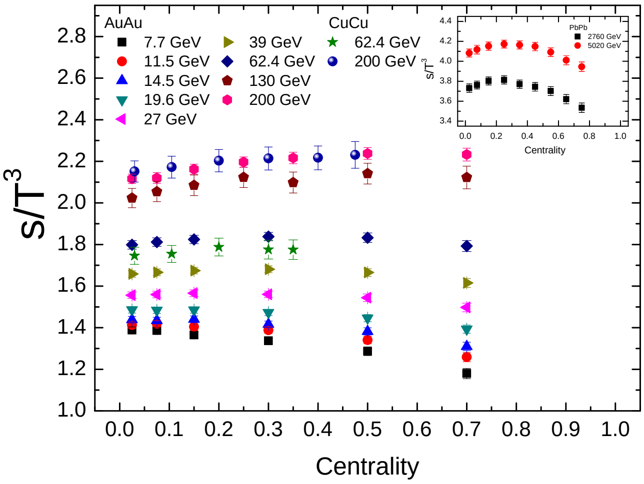

Fig. 4. (Color online) The scaled entropy density in the Au+Au collisions at $\sqrt{s_{\rm NN}} = 7.7 - 200$ GeV, and in the Cu+Cu collisions at $\sqrt{s_{\rm NN}} = 62.4, 200$ GeV, as a function of the centrality. The values are calculated using Eq. (9). The results for the Pb+Pb collisions are obtained from Ref. [24] and shown in the insert.

parameters were approximately the same when the collision centrality was the same. This can be indicated by the massless particle limit; the analytical formulas (Eqs. (13, 15)) of ε/T^4 and s/T^3 for the massless particles are proportional. Furthermore, the figure demonstrates that the difference in the values between the most central and peripheral collisions is subtle at high collision energies. This is reasonable because similar nuclear reaction environments are created at different centralities at higher collision energies.

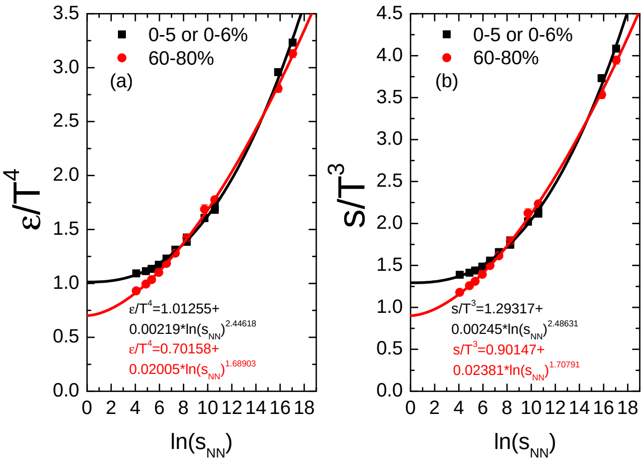

Fig. 5. (Color online) The scaled ε/T^4 and s/T^3 for the most central (black) collision and most peripheral (red) collision in the Au+Au collisions at $\sqrt{s_{\rm NN}} = 7.7 - 200$ GeV, and in the Cu+Cu collisions at $\sqrt{s_{\rm NN}} = 62.4, 200$ GeV, as a function of $\ln(s_{\rm NN})$. The lines are fitted with the expressions shown at the bottom of the figure. The parameters used to calculate the thermodynamic quantities for the Pb+Pb collisions are obtained from Ref. [24].

D. Particle density

The particle density in units of fm^{-3}, which was calculated as a function of the centrality using Eq. (8), is shown in Fig. 6. The particle density results for the Pb+Pb collisions at $\sqrt{s_{\rm NN}} = 2760, 5020$ GeV that were obtained from Ref. [24] are also plotted in the figure. The patterns of the dependence of the particle density on the collision energy, size of the collision system, and collision centrality are the same as those indicated in Fig. 2a and the pressure in Fig. 3a. See the explanation in Sect. III A for further details.

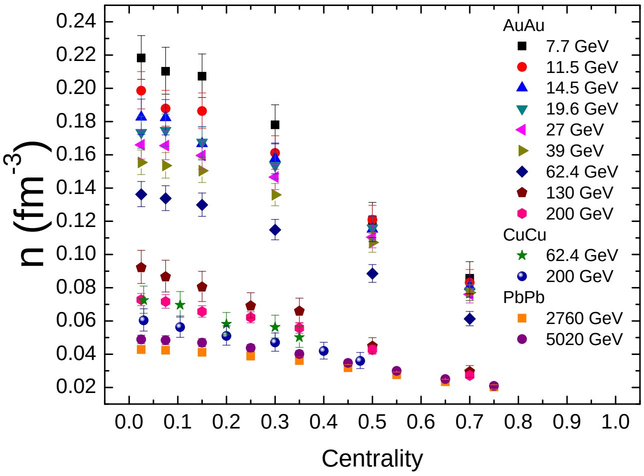

Fig. 6. (Color online) Particle density in the Au+Au collisions at $\sqrt{s_{\rm NN}} = 7.7 - 200$ GeV, and in the Cu+Cu collisions at $\sqrt{s_{\rm NN}} = 62.4, 200$ GeV, as a function of centrality. The values are calculated using Eq. (8). The results for the Pb+Pb collisions are obtained from Ref. [24].

IV. CONCLUSION

In this study, we used the thermodynamically consistent Tsallis distribution to fit the transverse momentum spectra of the charged particles from the Au+Au collisions at $\sqrt{s_{\rm NN}} = 7.7 - 200$ GeV, and the Cu+Cu collisions at $\sqrt{s_{\rm NN}} = 62.4, 200$ GeV [29–32] at the RHIC, and extracted the corresponding temperature parameter T and Tsallis parameter q. The Tsallis parameter q demonstrates an increasing trend with an increase in the collision energy and centrality, whereas the temperature parameter T demonstrates the opposite trend. Substituting T and q into the formulas for the thermodynamic quantities of the collision system at the kinetic freeze-out in the framework of the Tsallis statistics, the energy density ε, scaled energy density ε/T^4, scaled entropy density s/T^3, pressure P, squared speed of sound, and particle density of the charged particles were investigated. The errors propagated by the uncertainties of the fitting parameters were also considered. The results indicate that the energy density, pressure, and particle density exhibit decreasing trends with an increase in the collision energy for a given collision centrality. This can be explained

by the interplay between the total multiplicity of the charged particles produced in the collisions and the volume of the collision system. The three thermodynamic quantities also demonstrated a decreasing trend with an increase in the centrality for a given collision energy. The squared speed of sound obtained from the different collision centralities was nearly constant at the same collision energy and varied only within a significantly small range for all collision energies. Both the scaled ε/T^4 and s/T^3 increased as the collision energy increased and demonstrated a significantly weak dependence on the collision centrality. For the scaled energy and entropy densities, the size dependence of the collision system disappeared. The scaled ε/T^4 and s/T^3 demonstrated a similar behavior as a function of $\ln(s_{\rm NN})$ for a given collision centrality, which can be understood by the analytical formulas of Eqs. (13) and (15). This study complements the work in Ref. [24]. In future work, we will study the thermodynamic quantities at the chemical freeze-out and investigate their evolution in the hadronic phase from the chemical to kinetic freeze-out at the RHIC and LHC.

Author contributions All authors contributed to the study conception and design. Material preparation, data collection and analysis were performed by Wei-Hao Wu, Jun-Qi Tao, Hua Zheng, Wen-Chao Zhang, Xing-Quan Liu, Li-lin Zhu and Aldo Bonasera. The first draft of the manuscript was written by Wei-Hao Wu and Hua Zheng and all authors commented on previous versions of the manuscript. All authors read and approved the final manuscript.

Data Availability The data that support the findings of this study are openly available in Science Data Bank at https://www.doi.org/10.57760/sciencedb.j00186.00239 and https://cstr.cn/31253.11.sciencedb.j00186.00239.

[1] C.Y. Wong, *Introduction to High-Energy Heavy-Ion Collisions*, 1st ed., World Scientific: Singapore, 1994.

[2] Edited by R.C. Hwa and X.N. Wang, *Quark-Gluon Plasma 3*. World Scientific, Singapore, 2004.

[3] Edited by R.C. Hwa and X.N. Wang, *Quark-Gluon Plasma 4*. World Scientific, Singapore, 2010.

[4] X. Luo and N. Xu, Search for the QCD Critical Point with Fluctuations of Conserved Quantities in Relativistic Heavy-Ion Collisions at RHIC : An Overview. Nucl. Sci. Tech. **28**, 112 (2017). https://doi.org/10.1007/s41365-017-0257-0

[5] C.M. Ko, Searching for QCD critical point with light nuclei. Nucl. Sci. Tech. **34**, 80 (2023). https://doi.org/10.1007/s41365-023-01231-1

[6] J. Chen, D. Keane, Y. G. Ma, A. Tang and Z. Xu, Antinuclei in Heavy-Ion Collisions, Phys. Rept. **760**, 1-39 (2018). https://doi.org/10.1016/j.physrep.2018.07.002

[7] H. X. Zhang, Y. X. Xiao, J. W. Kang and B. W. Zhang, Phenomenological study of the anisotropic quark matter in the two-flavor Nambu–Jona–Lasinio model, Nucl. Sci. Tech. **33**, 150 (2022). https://doi.org/10.1007/s41365-022-01129-4

[8] M. Wang, J. Q. Tao, H. Zheng, W. C. Zhang, L. L. Zhu and A. Bonasera, Number-of-constituent-quark scaling of elliptic flow: a quantitative study, Nucl. Sci. Tech. **33**, 37 (2022). https://doi.org/10.1007/s41365-022-01019-9

[9] B.I. Abelev, *et al.* (STAR Collaboration). Systematic measurements of identified particle spectra in pp, $d+$ Au, and Au $+$ Au collisions at the STAR detector. Phys. Rev. C **79**, 034909 (2009). https://doi.org/10.1103/PhysRevC.79.034909

[10] L. Adamczyk, *et al.* (STAR Collaboration). Bulk properties of the medium produced in relativistic heavy-ion collisions from the beam energy scan program. Phys. Rev. C **96**, 044904 (2017). https://doi.org/10.1103/PhysRevC.96.044904

[11] Y.Q. Gao, C.X. Tian, M.Y. Duan, B.C. Li, F.H. Liu. Transverse momentum distributions of identified particles produced in pp, p(d), and AA collisions at high energies. Pramana. J. Phys. **79**, 1407 (2012). https://doi.org/10.1007/s12043-012-0350-1

[12] F.H. Liu, Y.Q. Gao, T. Tian, C.B. Li. Unified description of transverse momentum spectrums contributed by soft and hard processes in high-energy nuclear collisions. Eur. Phys. J. A **50**, 94 (2014). https://doi.org/10.1140/epja/i2014-14094-9

[13] E. Schnedermann, J. Sollfrank, U. Heinz. Thermal phenomenology of hadrons from 200A GeV S + S collisions. Phys. Rev. C **48**, 2462 (1993). https://doi.org/10.1103/PhysRevC.48.2462

[14] C. Y. Wong and G. Wilk, Tsallis Fits to p_T Spectra for pp Collisions at LHC, Acta Phys. Polon. B **43**, 2047-2054 (2012). https://doi.org/10.5506/APhysPolB.43.2047

[15] C. Y. Wong and G. Wilk, Tsallis fits to p_T spectra and multiple hard scattering in pp collisions at the LHC, Phys. Rev. D **87**, 114007 (2013). https://doi.org/10.1103/PhysRevD.87.114007

[16] R.N. Patra, B. Mohanty, T.K. Nayak, Centrality, transverse momentum and collision energy dependence of the Tsallis parameters in relativistic heavy-ion collisions. Eur. Phys. J. Plus. **136**, 702 (2021). https://doi.org/10.1140/epjp/s13360-021-01660-0

[17] M.D. Azmi, J. Cleymans. The Tsallis distribution at large transverse momenta. Eur. Phys. J. C **75**, 430 (2015). https://doi.org/10.1140/epjc/s10052-015-3629-9

[18] L. Marques, J. Cleymans, A. Deppman. Description of high-energy pp collisions using Tsallis thermodynamics: Transverse momentum and rapidity distributions. Phys. Rev. D **91**, 054025 (2015). https://doi.org/10.1103/PhysRevD.91.054025

[19] K. Saraswat, P. Shukla, V. Singh. Transverse momentum spectra of hadrons in high energy pp and heavy ion collisions. J. Phys. Commun. **2**, 035003 (2018). 10.1088/2399-6528/aab00f

[20] J. Cleymans, D. Worku. The Tsallis distribution in proton–proton collisions at $\sqrt{s}$ = 0.9 TeV at the LHC. J. Phys. G: Nucl. Part. Phys. **39**, 025006 (2012). 10.1088/0954-3899/39/2/025006

[21] J. Cleymans, D. Worku. Relativistic thermodynamics: Transverse momentum distributions in high-energy physics. Eur. Phys. J. A **48**, 160 (2012). https://doi.org/10.1140/epja/i2012-12160-0

[22] J. Cleymans, M.D. Azmi, A.S. Parvan et al., The Parameters of The Tsallis Distribution at the LHC. EPJ Web of Conf. **137**, 11004 (2017). https://doi.org/10.1051/epjconf/201713711004

[23] A.S. Parvan, O.V. Teryaev, J. Cleymans. Systematic comparison of Tsallis statistics for charged pions produced in pp collisions. Eur. Phys. J. A **53**, 102 (2017). https://doi.org/10.1140/epja/i2017-12301-y

[24] M.D. Azmi, T. Bhattacharyya, J. Cleymans, M. Paradza. Energy density at kinetic freeze-out in Pb–Pb collisions at the LHC using the Tsallis distribution. J. Phys. G: Nucl. Part. Phys.

47, 045001 (2020). 10.1088/1361-6471/ab6c33

[25] J.Q. Tao, W.H. Wu, M. Wang, H. Zheng, W.C. Zhang, L.L. Zhu, A. Bonasera. The Novel Scaling of Tsallis Parameters from the Transverse Momentum Spectra of Charged Particles in Heavy-Ion Collisions. Particles **5**, 146-156 (2022). https://doi.org/10.3390/particles5020013

[26] P.K. Khandai, P. Sett, P. Shukla, V. Singh. Hadron Spectra in p + p Collisions at RHIC and LHC Energies. Int. J. Mod. Phys. A **28**, 1350066 (2013). https://doi.org/10.1142/S0217751X13500668

[27] H. Zheng, L.L. Zhu. Can Tsallis Distribution Fit All the Particle Spectra Produced at RHIC and LHC?. Adv. High Energy Phys. **2015**, 180491 (2015). https://doi.org/10.1155/2015/180491

[28] X.J. Yin, L.L. Zhu, H. Zheng. A New Two-Component Model for Hadron Production in Heavy-Ion Collisions. Adv. High Energy Phys. **2017**, 6708581 (2017). https://doi.org/10.1155/2017/6708581

[29] L. Adamczyk, *et al.* (STAR Collaboration). Beam Energy Dependence of Jet-Quenching Effects in Au + Au Collisions at $\sqrt{s_{\rm NN}}$ = 7.7, 11.5, 14.5, 19.6, 27, 39, and 62.4 GeV. Phys. Rev. Lett. **121**, 032301 (2019). https://doi.org/10.1103/PhysRevLett.121.032301

[30] C. Adler, *et al.* (STAR Collaboration). Centrality Dependence of High-p_T Hadron Suppression in Au + Au Collisions at $\sqrt{s_{NN}}$ = 130 GeV. Phys. Rev. Lett. **89**, 202301 (2002). https://doi.org/10.1103/PhysRevLett.89.202301

[31] J. Adams, *et al.* (STAR Collaboration). Transverse-Momentum and Collision-Energy Dependence of High-p_T Hadron Suppression in Au + Au Collisions at Ultrarelativistic Energies. Phys. Rev. Lett. **91**, 172302 (2003). https://doi.org/10.1103/PhysRevLett.91.172302

[32] B. Alver, *et al.* (PHOBOS Collaboration). System Size and Centrality Dependence of Charged Hadron Transverse Momentum Spectra in Au + Au and Cu + Cu Collisions at $\sqrt{s_{NN}}$ = 62.4 and 200 GeV. Phys. Rev. Lett. **96**, 212301 (2006). https://doi.org/10.1103/PhysRevLett.96.212301

[33] B. Alver, *et al.* (PHOBOS Collaboration). Identified charged antiparticle to particle ratios near midrapidity in Cu+Cu collisions at $\sqrt{s_{NN}}$ = 62.4 and 200 GeV. Phys. Rev. C **77**, 061901 (2008). https://doi.org/10.1103/PhysRevC.77.061901

[34] C. Tsallis. Possible Generalization of Boltzmann-Gibbs Statistics. J. Statist. Phys. **52**, 479–487 (1988). https://doi.org/10.1007/BF01016429

[35] Y. Gao, H. Zheng, L.L. Zhu, A. Bonasera. Description of charged particle pseudorapidity distributions in Pb+Pb collisions with Tsallis thermodynamics. Eur. Phys. J. A **53**, 197 (2017). https://doi.org/10.1140/epja/i2017-12397-y

[36] J.Q. Tao, M. Wang, H. Zheng, W.C. Zhang, L.L. Zhu, A. Bonasera. Pseudorapidity distributions of charged particles in pp($\bar{p}$), p(d)A and AA collisions using Tsallis thermodynamics. J. Phys. G: Nucl. Part. Phys. **48**, 105102 (2021). 10.1088/1361-6471/ac1393

[37] J. Adams, *et al.* (STAR Collaboration). Bulk properties of the system formed in Au + Au collisions at $\sqrt{s_{NN}}$ = 14.5 GeV at the BNL STAR detector. Phys. Rev. C **101**, 024905 (2020). https://doi.org/10.1103/PhysRevC.101.024905

[38] A. Khuntia, P. Sahoo, P. Garg, R. Sahoo, J. Cleymans. Speed of sound in hadronic matter using non-extensive Tsallis statistics. Eur. Phys. J. A **52**, 292 (2016). https://doi.org/10.1140/epja/i2016-16292-9

[39] T. Bhattacharyya, J. Cleymans, S. Mogliacci. Analytic results for the Tsallis thermodynamic variables. Phys. Rev. D **94**, 094026 (2016). https://doi.org/10.1103/PhysRevD.94.094026

[40] H. Zheng, L.L. Zhu, A. Bonasera. Systematic analysis of hadron spectra in $p + p$ collisions using Tsallis distributions. Phys. Rev. D **92**, 074009 (2015). https://doi.org/10.1103/PhysRevD.92.074009

[41] H. Zheng, L.L. Zhu. Comparing the Tsallis Distribution with and without Thermodynamical Description in $p + p$ Collisions. Adv. High Energy Phys. **2016**, 9632126 (2016).https://doi.org/10.1155/2016/9632126

[42] H. Zheng, X. Zhu, L.L. Zhu, A. Bonasera. Systematic investigation of the particle spectra in heavy-ion collisions at the Large Hadron Collider. Mod. Phys. Lett. A **35**, 2050177 (2020). https://doi.org/10.1142/S0217732320501771

[43] E. Shuryak. Strongly coupled quark-gluon plasma in heavy ion collisions. Rev. Mod. Phys. **89**, 035001 (2017). https://doi.org/10.1103/RevModPhys.89.035001

[44] C.J. Zhang, J. Xu. Effects of hadronic mean-field potentials on Hanbury-Brown–Twiss correlations in relativistic heavy-ion collisions. Phys. Rev. C **96**, 044907 (2017). https://doi.org/10.1103/PhysRevC.96.044907